PHYSICAL REVIEW B **69**, 134417 (2004)

Critical scattering of polarized neutrons in the invar $Fe_{65}Ni_{35}$ alloy

S. V. Grigoriev,[1,3,*] S. V. Maleyev,[1] A. I. Okorokov,[1] H. Eckerlebe,[2] and N. H. van Dijk[3]
[1]*Petersburg Nuclear Physics Institute, Gatchina, St. Petersburg 188350, Russia*
[2]*GKSS Forchungszentrum, 21502 Geesthacht, Germany*
[3]*Interfacultair Reactor Instituut, TU Delft, 2629 JB Delft, The Netherlands*
(Received 12 April 2003; revised manuscript received 13 October 2003; published 14 April 2004)

The magnetic phase transition in the invar $Fe_{65}Ni_{35}$ alloy has been investigated by small-angle polarized-neutron scattering (SAPNS) along with both three-dimensional neutron depolarization and thermal-expansion measurements. The data give evidence for a smeared phase transition. A spatial distribution in the Curie temperature T_C is introduced to explain the experimental data. The local T_C variations are described by the standard deviation of the transition temperature ΔT_C and by the characteristic length of the T_C variations, R_0. The deduced parameters are $\langle T_C\rangle = 485 \pm 0.5$ K, $\Delta T_C = 12.5 \pm 0.2$ K, and $R_0 \approx 300$ nm. The critical SAPNS experiment was performed in a special inclined geometry ($\vec{H}$ is inclined to the wave vector $\vec{k}$). Two different contributions to the critical scattering were analyzed in the magnetic-field range (1–1000 G) and the temperature range ($T_C \pm 0.1 T_C$) of interest. First, the two-spin-correlation function was studied. Second, the dynamical three-spin-correlation function, or the so-called dynamical chirality of the system, was investigated by extracting the asymmetric part of the polarization-dependent scattering. We distinguish two contributions in the chiral scattering, which stem from the spin waves in the large magnetic inhomogeneities and from the three-spin-correlation function of the critical fluctuations. The data are interpreted in terms of the static and dynamic scaling theory accounting for the concept of local T_C variations.

DOI: 10.1103/PhysRevB.69.134417 PACS number(s): 61.12.Ex, 75.40.−s, 75.50.Bb

I. INTRODUCTION

The magnetic phase transition in disordered systems has recently attracted much attention. In the last decade the problem of a coexistence of two length scales for the fluctuations of the order parameter above the phase-transition temperature T_C was extensively studied[1] and both large-scale fluctuations and critical fluctuations on a small length scale were observed. In spite of the fact that observation of the ''two-scale'' phenomenon had been made in pure materials, the appearance of the large-scale fluctuations is attributed to disorder in the system.[2] The mechanism of this phenomenon is not clarified yet. On the other hand, attempts have been made to describe the experimental data in disordered systems using a scaling theory with a Gaussian distribution for the transition temperature.[3–5] Recently it was suggested[6,7] that the presence of spatial variations in T_C is closely related to the enhancement of the large-scale fluctuations above T_C.

In previous works[8,9] we concluded from neutron depolarization (ND) and small-angle neutron-scattering (SANS) measurements that two different length scales for the magnetic correlations coexist in invar FeNi alloys around the mean critical temperature $\langle T_C\rangle$. Using SANS it was shown that the smaller length scale is attributed to the critical fluctuations and that their shape is well described by a Lorentzian in reciprocal space. Using neutron depolarization much larger magnetic inhomogeneities were found above T_C. Their shape could be roughly modeled by a squared Lorentzian. Recently, the presence of two length scales above $\langle T_C\rangle$ was interpreted as a consequence of the large-scale disorder, which leads to local variations in T_C.[6,7,10] These local T_C variations are described by the average Curie temperature $\langle T_C\rangle$, its spread ΔT_C, and the characteristic size R_0 of the areas with different T_C. In Refs. 6, 7, and 10 a model was proposed to describe the influence of the large-scale disorder on the ferromagnetic transition. In general, the scaling theory of a second-order phase transition assumes only one length scale, which determines the properties of the system near the phase transition. This is the correlation length of the order parameter describing the critical fluctuations $R_c = a\tau^{-\nu}$, where $\tau = (T - T_C)/T_C$ is the reduced temperature, $\nu \simeq 2/3$ is a critical exponent, and a is of the order of the lattice constant. When T_C variations, characterized by $\tau_1 = \Delta T_C/\langle T_C\rangle$, are relatively large, then they cause the appearance of another characteristic length scale R_0. The ferromagnetic transition can then have a complex (inhomogeneous) nature. We consider two limiting cases. When the length scale R_0 is much smaller than R_c at $\tau = \tau_1$, then the thermal fluctuations average out the locally disordered regions. This leads to the homogeneous scenario of the phase transition. In contrary, when $R_0 \gg R_c(\tau_1)$, the thermal fluctuations do not average out the local variations in T_C that leads to a percolative (or inhomogeneous) scenario for the transition.[6,7] In a previous study we used the three-dimensional (3D) neutron depolarization technique to investigate the large scale correlations near $\langle T_C\rangle$ in an invar $Fe_{70}Ni_{30}$ alloy doped with 0.7 at. % carbon.[9] We interpreted the data of the ND experiment in terms of an appearance of large-scale magnetic inhomogeneities above T_C. The characteristic parameters derived for the ferromagnetic phase transition of $Fe_{70}Ni_{30}$ are $\langle T_C\rangle = 397$ K, $\Delta T_C = 4.5$ K, and $R_0 \approx 10^3$ nm.

In the present paper we continue investigation of the ferromagnetic phase transition in the classical invar $Fe_{65}Ni_{35}$ alloy. This alloy shows similar features as the $Fe_{75}Ni_{25}$ and $Fe_{70}Ni_{30}$ alloys, investigated in Refs. 8 and 9. The magneti-

zation and neutron depolarization were measured as a function of temperature at different magnetic fields. We fitted the temperature dependence of the magnetization by a convolution of the distribution function $\rho(T_C)$ and the scaling law for the magnetization. The same analysis was performed on the data from ND measurements leading to additional results on the scale parameter of the disorder R_0. The deduced parameters are $\langle T_C\rangle = 485 \pm 0.5$ K, $\Delta T_C = 12.5 \pm 0.2$ K, and $R_0 \approx 300$ nm. We have complemented the data of the neutron depolarization with thermal-expansion (TE) measurements. These data show changes in the sample length near the ferromagnetic transition caused by a strong spin lattice coupling in the vicinity of T_C. The latter combined with concentration inhomogeneities in the alloy may be pointed as a possible origin for the observed T_C variations.

Furthermore, the paper is aimed to study the effect of T_C variations on static and dynamic properties of the magnetic system on the length scale of the critical fluctuations. For this reason small-angle polarized neutron-scattering (SAPNS) experiments were performed in a magnetic field $\vec{H}$ inclined to the wave vector $\vec{k}$. This geometry allows one to distinguish three contributions to the critical scattering. First, the pair-correlation function, which is related to that part of the scattering which may be studied by non-polarized SANS. This contribution does not depend on the polarization. Second, the nuclear-magnetic cross correlation, or the interference, term is attributed to the symmetric polarization-dependent part of the scattering. This contribution appears when fluctuations of the nuclear and magnetic contrasts occur at the same (r,t) space. Third, the dynamical three-spin-correlation term contributes to the asymmetric polarization-dependent part of SAPNS. This term is a projection of the chiral spin fluctuations onto the sample magnetization and is known as a dynamical chirality. One may extract and investigate this part only if an inclined geometry is used.[11–13] In this method one measures the left-right asymmetry in the SAPNS pattern that originates from the interaction of the neutron spin with the dynamic three-spin correlation. Later on this method was extended to investigate the spin-wave dynamics in ferromagnets.[14–16] The pair spin-correlation function is studied as a function of the temperature and the magnetic field. A crossover to the strong-field regime in the critical temperature range is observed. We distinguished and separated two contributions in the asymmetric scattering, which stem from the spin waves in the large magnetic inhomogeneities and from the three-spin-correlation function in the critical fluctuations. The existence of spin waves is observed in the temperature range $T_C - \Delta T_C < T < T_C + \Delta T_C$, where both ferromagnetic and paramagnetic regions coexist. The temperature behavior of the spin-wave scattering intensity is found to be proportional to $\langle S\rangle T$ convoluted with the distribution function $\rho(T_C)$ with $\langle S\rangle$ as an average spin. Another contribution to the inelastic scattering is that of the three-spin-correlation function. It depends linearly on the magnetic field and has the same q dependence as the pair correlation. This behavior is in agreement with the principle of the dynamical critical factorization,[17] which is known as Poliakov-Kadanoff-Wilson algebra.

The paper is organized in the following way. Section II gives a description of the magnetic phase transition with a Gaussian distribution of the variations in T_C. This section contains the data of the three-dimensional analysis interpreted in terms of the concept of T_C variations. The data of TE is added into the section for completeness. The results of the SAPNS measurements are given in Sec. III. There we show what information can be obtained from the SAPNS in the so-called inclined geometry. The temperature and magnetic-field dependence of the different contributions to the SAPNS pattern are shown and the parameters extracted after the fitting procedure are discussed there. The theoretical background describing SAPNS in inclined geometry is explained in the Appendix.

II. MAGNETIC PHASE TRANSITION WITH GAUSSIAN DISTRIBUTION FOR THE T_C VARIATIONS

A. The concept

We assume the presence of local T_C variations in our invar iron-nickel alloys.[4,5,8,9] As shown below, this assumption is confirmed by experimental data. Let us consider the presence of T_C variations with a Gaussian distribution:

$$\rho(T_C) = \frac{1}{\sqrt{2\pi(\Delta T_C)^2}} \exp\left(- \frac{(T_C - \langle T_C\rangle)^2}{2\Delta T_C^2} \right), \qquad (1)$$

where $\langle T_C\rangle$ is the average Curie temperature and ΔT_C is its spread. In accordance with Refs. 6, 7, and 10 the concept implies the introduction of a characteristic length scale R_0 corresponding to the correlation length of the T_C variations. Indeed, the Curie temperature is, by definition, a macroscopic parameter of the material. The length scale R_0 for the variations in T_C, therefore, has to be much larger than the correlation length of the critical fluctuations R_C. As was shown in Refs. 6, 7, and 10, the relatively large T_C variations, $\tau_1 = \Delta T_C / \langle T_C\rangle$ combined with their large correlation length R_0, result in a ferromagnetic transition with a percolative (inhomogeneous) rather than a homogeneous nature. Rigorously speaking, if the spatial variation R_0 of T_C is larger than the correlation length $a(\langle T_C\rangle/\Delta T_C)^{\nu}$, one should take into account the spread of T_C. In other limiting case $R_0 < a(\langle T_C\rangle/\Delta T_C)^{\nu}$ it has to be neglected.

The qualitative description of this percolative transition can be given as follows. The magnetic state of the system for the temperatures around $\langle T_C\rangle$ can be described as ferromagnetic droplets in a paramagnetic matrix with critical fluctuations both in the ferromagnetic and paramagnetic regions. The heavily damped spin waves are enhanced in the ferromagnetic regions. These locally ordered magnetic regions grow in the paramagnetic phase and tend to form a large percolating cluster at $\langle T_C\rangle$. In zero field above $\langle T_C\rangle$ the direction of the magnetization in the ferromagnetic clusters is random, so that the average magnetization is equal to zero. Nevertheless, in an applied magnetic field the magnetic moments of these locally ordered regions have to be aligned. Then a mean magnetic induction, composed of the magnetic moments in the locally ordered clusters, appears as a response to the external magnetic field.

B. Method: Neutron depolarization

The three-dimensional neutron depolarization technique gives the information on the average magnetic induction and the average size of the magnetic inhomogeneities/domains. In this technique the polarized-neutron beam is transmitted through the sample. The polarization of the neutron beam, $\vec{P}$, changes after transmission. This change involves both a precession of the polarization vector, due to the average magnetic induction in the sample $\langle \mathbf{B}(\mathbf{r}) \rangle$, and a reduction of its length, i.e., a decrease of the degree of polarization, due to fluctuations of the magnetic induction $\Delta \mathbf{B}(\mathbf{r}) = \mathbf{B}(\mathbf{r}) - \langle \mathbf{B} \rangle$. The rotation angle ϕ of the polarization vector around the average magnetic induction $\langle B \rangle$ can be expressed as $\phi = \sqrt{c} \langle B \rangle L$, where L is the sample thickness, $c = 2.15 \times 10^{29} \lambda^2$ m^{-4} T^{-2}, and λ is the neutron wavelength. Thus the magnetic induction $\langle B \rangle$ can be directly derived from the measured value of the rotation angle ϕ. The reduction in $|\mathbf{P}|$ (depolarization) is related to the fluctuations in the local magnetic induction $\Delta \mathbf{B}$ by $(|\mathbf{P}|/|\mathbf{P}_0|) = \exp[-\alpha c R_d \langle (\Delta \mathbf{B})^2 \rangle L]$, where R_d is the average size of the large-scale magnetic inhomogeneities/domains/clusters, and $\alpha \sim 1$ is a constant depending on the mutual orientation of the initial polarization $\mathbf{P}_0$, and the neutron wave vector $\mathbf{k}$, and $\langle \mathbf{B} \rangle$.[18–20] Provided ΔB is known, one can obtain the average size of the magnetic inhomogeneities R_d by measuring the degree of the polarization P/P_0. It should be noticed that the neutron depolarization strongly depends on the neutron wavelength λ, which determines the sensitivity range of the measurements. If $\lambda = 0.1$ nm, then for a typical sample thickness $L = 1$ mm, we can expect 1% of depolarization for magnetic inhomogeneities with a strength of $B = 1$ kG and a size of $R_d = 10^3$ nm. If $\lambda = 1$ nm, then the sensitivity of the method increases by factor 100 and consequently the magnetic inhomogeneities of $R_d \approx 10$ nm become visible.

In the same way as shown in Ref. 9 for $Fe_{70}Ni_{30}$ we use the three-dimensional analysis of the neutron depolarization to study the magnetic state of $Fe_{65}Ni_{35}$ as a function of the temperature and the magnetic field. A plate with dimensions $40 \times 10 \times 1.0$ mm^3 was used as a sample, where $L = 1.0$ mm is the transmission length and the field was oriented along the long axis, i.e., perpendicular to the beam. Three-dimensional neutron depolarization experiments were performed on the instrument PANDA at IRI in Delft. A neutron beam was monochromatized at $\lambda = 0.124$ nm ($\Delta\lambda/\lambda = 0.02$) and polarized with a degree of polarization $P_0 = 0.94$. The sample was mounted into a furnace that could be regulated within 0.1 K for temperatures from 300 K up to 700 K. The applied magnetic field was changed in the range from 0 to 50 G. In order to extend the sensitivity of the method the depolarization data were also taken at $\lambda = 0.92$ nm ($\Delta\lambda/\lambda = 0.2$) on the instrument Vector at the WWR-M reactor at St Petersburg Nuclear Physics Institute.[21]

C. Results: Neutron depolarization

The rotation angle ϕ and the degree of polarization of the transmitted neutron beam $|P/P_0|$ were measured as a function of the temperature near $\langle T_C \rangle \approx 485$ K at different values of the applied magnetic field: $H = 0,5,10,20,30,40,50$ G. Figure 1 shows the values of ϕ and $|P/P_0|$ as a function of the field at different temperatures near the phase transition. As can be seen in Fig. 1, the magnetic moment of these locally ordered regions tends to align in the applied magnetic field. The magnetic induction $\langle B \rangle$ grows rapidly with H and saturates in a magnetic field of 40–50 G. In comparison, the depolarization shows a weak-field dependence only. From this we conclude that the applied magnetic field is sufficiently strong to move the domain walls inside the ferromagnetic regions, but is weak in comparison with the anisotropy field. So, when a magnetic field of 50 G is applied, almost all magnetic clusters are oriented along the preferred local anisotropy axis through the whole critical temperature range.

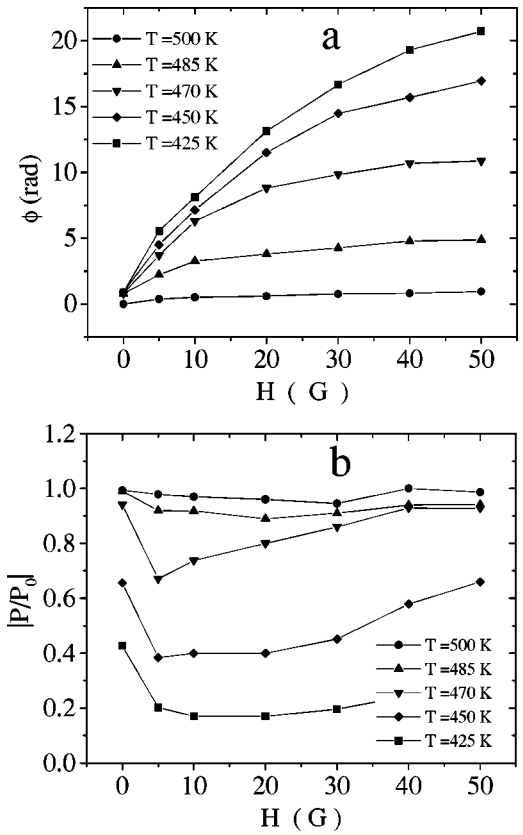

FIG. 1. The magnetic-field dependence of the polarization rotation angle ϕ (a) and the neutron polarization $|P/P_0|$ (b).

The temperature dependence of ϕ at $H = 50$ G was analyzed using the Gaussian probability function $\rho(T_C)$ for the variations in the Curie temperature T_C with an average value $\langle T_C \rangle$ and with the standard deviation ΔT_C [Eq. (1)]. Furthermore, we suppose that the local magnetic induction inside the inhomogeneities is described by the scaling law $B(T, T_C) = A\tau^\beta$ for $T \leqslant T_C$ with a reduced temperature $\tau = (T_C - T)/T_C$ and a critical exponent of $\beta = 0.37$ corresponding to a pure ferromagnet. The rotation angle $\phi(T)$ can be expressed by the convolution of $B(T, T_C)$ and $\rho(T_C)$:

$$\phi(T) = \sqrt{c} L \int_T^\infty \rho(T_C) B(T, T_C) dT_C . \qquad (2)$$

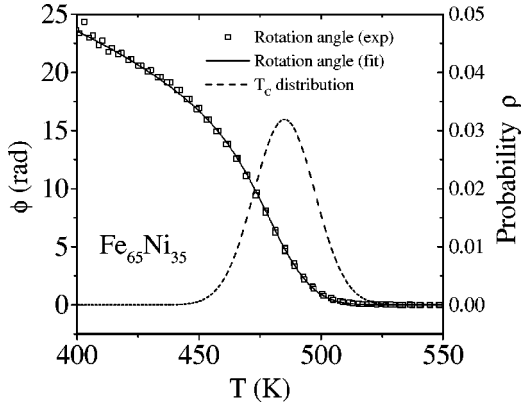

FIG. 2. The temperature dependence of the measured and fitted rotation angle ϕ with the corresponding distribution function of T_C.

Figure 2 shows the experimental data of the rotation angle in an applied magnetic field of 50 G (closed squares) and the fit to Eq. (2) (solid line). The experimental data of $\phi(T)$ were fitted by Eq. (2) using the least-squares method. We find $\langle T_C\rangle = 485 \pm 0.5$ K, $\Delta T_C = 12.5 \pm 0.2$ K, and $A = 0.87 \pm 0.02$ T.

The temperature dependence of the polarization of the transmitted beam $|P/P_0|$ is shown in Fig. 3(a) for $H=0$ at a wavelength $\lambda = 0.124$ nm and 0.92 nm. At $T \gg T_C$ the polarization of the transmitted beam is close to the incident polarization P_0. When during cooling the temperature approaches the transition region, the depolarization appears at $T \approx 500$ K. This demonstrates an increase of the magnetic correlation length and the magnetization inside magnetic inhomogeneities. According to the previous discussion the neutron depolarization can be attributed to the appearance of magnetic inhomogeneities with $B \approx 10^2 - 10^3$ G and a size of about $10^2 - 10^4$ nm.

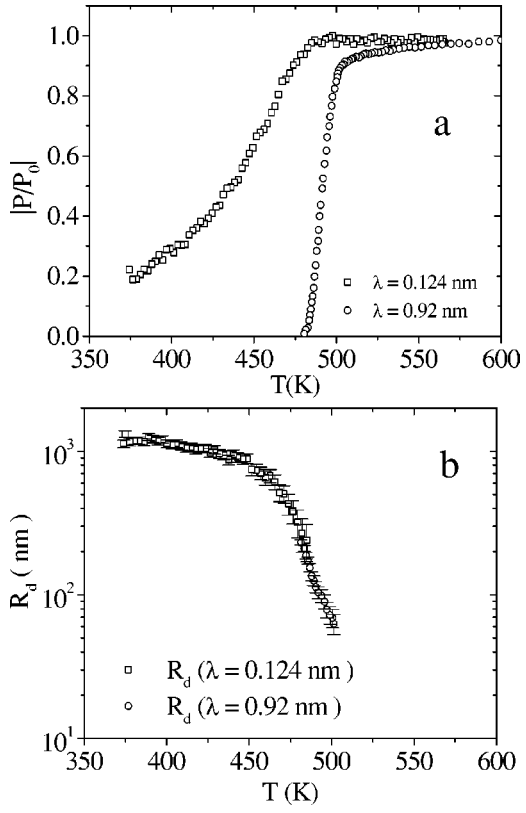

FIG. 3. The temperature dependence of the neutron depolarization $|P/P_0|$ at different values of the wavelength $\lambda = 0.124$ nm and $\lambda = 0.92$ nm (a) and the average size of the magnetic inhomogeneities R_d (b).

As was discussed above, the signal $\ln(|P/P_0|)$ scales with λ^2. A different sensitivity of this method for a different wavelength is clearly seen in Fig. 3(a). For $\lambda = 0.124$ nm the magnetic inhomogeneities at $T > 480$ K are too small and therefore invisible. At $T < 480$ K they are rather large and partially depolarize the neutron beam. For $\lambda = 0.92$ nm the neutron beam is fully depolarized for $T < 480$ K and therefore the information on the magnetic inhomogeneities is lost. The polarization $|P/P_0|$ changes drastically from 0 to 0.9 in the temperature range from 480 K to 500 K showing the presence of the magnetic inhomogeneities at this temperature range.

The temperature dependence of the polarization $|P/P_0|$ may be also interpreted in terms of a Gaussian distribution in T_C. In analogy with Eq. (2) the polarization can be expressed as

$$|P(T)/P_0| = \exp\left(-cLR_d(T) \int_T^\infty \rho(T_C) B^2(T, T_C) dT_C \right). \tag{3}$$

To obtain the value of the size R_d from the neutron depolarization data we take for $\rho(T_C)$ and $B(T, T_C)$ parameters derived from the fit of $\phi(T)$. Figure 3(b) shows the derived temperature dependence of R_d. The combined data taken at different values of the neutron wavelength used to cover the large range of the depolarizing magnetic inhomogeneities from $R_d \approx 60$ nm to 2×10^3 nm. As seen from Fig. 3(b), the characteristic size of magnetic inhomogeneities grows with decreasing temperature in the range from $T \approx 500$ K to 450 K. The size R_d stays almost constant below $T = 450$ K. This plot may be interpreted as a formation of domains with a stable size of the order of $1-2$ μm below 450 K. The drastic change in the size as a function of T is related to a change in the magnetic clusters at the magnetic phase transition. We find that at $T \approx \langle T_C \rangle$ the correlation length of the T_C variations amounts to $R_d(T_C) \approx 300$ nm.

D. Thermal-expansion measurement

It is well known that the iron-nickel alloys were named invars after the discovery of its anomalously small value of the thermal-expansion coefficient in a wide temperature range. The correlation between spin and lattice systems had been established by a simple observation of the coincidence of the Curie temperature and the temperature where an unusual invar behavior starts to reveal itself. To investigate the invar properties of the sample we performed the TE measurements of the relative length of the sample $(\Delta L/L)$ as a function of the temperature [Fig. 4(a)]. The TE measure-

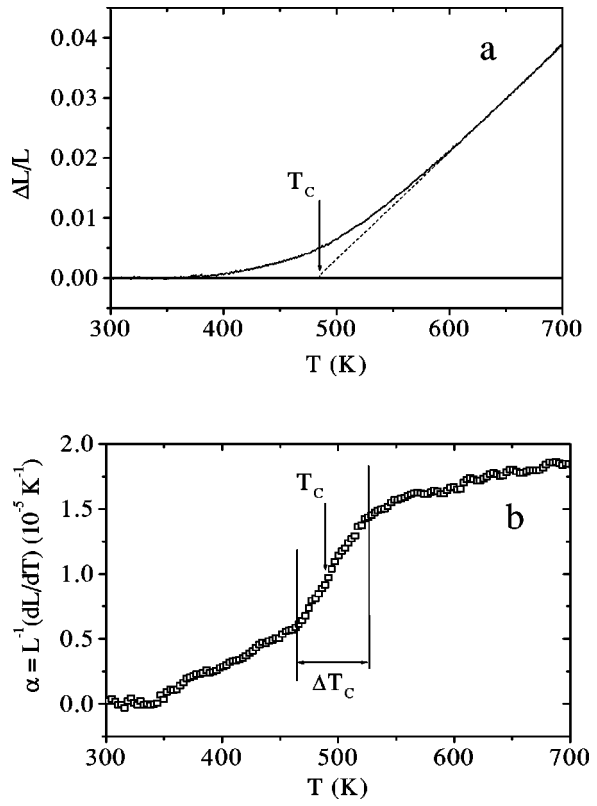

FIG. 4. The temperature dependence of the relative length of the sample $(\Delta L/L)$ (a) and the thermal-expansion coefficient $\alpha = (1/L)(dL/dT)$ (b).

ments were performed on a commercial Bähr805 dilatometer. The thermal-expansion coefficient $\alpha = (1/L)(dL/dT)$ is shown in the same picture [Fig. 4(b)]. In order to illustrate the temperature range, where the invar transition occurs, we make a simple linear extrapolation of the relative length change $\Delta L/L$ from the high- and from the low-temperature ranges [see Fig. 4(a)]. This rough extrapolation gives the crossover temperature at $T = 483 \pm 2$ K. This crossover temperature is in good agreement with the Curie temperature of $T_C = 485$ K obtained by the three-dimensional neutron depolarization measurements. The thermal-expansion coefficient α exhibits drastic changes in the temperature range from $T \approx 470$ to 530 K. Below $T = 470$ K the value of α decreases smoothly and it nearly vanishes at room temperature. Although such a behavior of the thermal-expansion coefficient is in agreement with the textbooks (see, for example, Ref. 22), it is interesting to find a correspondence between changes of the spin and lattice systems of invar near T_C. The appearance of the magnetic phase is described by the probability function centered at $T = 485$ K with half-width of 12.5 K. Thus the lower boundary of the magnetic transition $T_L = 485\text{-}12.5 \approx 470$ K coincides with that of the change of α [Fig. 4(b)]. However, the upper boundary of the transition $T_{UP} = 485 + 12.5 \approx 500$ K is 30 K lower than the temperature where a drop in α starts [Fig. 4(b)]. The change in α in the temperature range from 500 to 530 K may be only attributed to the appearance of the critical fluctuations of the magnetization. Therefore we should conclude that the spin and lattice systems are coupled not only in the ferromagnetic phase below T_C but also in the paramagnetic phase above T_C inside the magnetic critical region.

III. CRITICAL SCATTERING OF POLARIZED NEUTRONS

A. Method and experiment

Small-angle neutron scattering is a powerful tool to investigate the critical phenomena in ferromagnets. In general, the scattering cross section for polarized neutrons consists of four terms: nuclear σ_N, magnetic σ_M, nuclear-magnetic interference σ_I, and chiral σ_{CH} terms.[23,24] The first two terms do not depend on the incident polarization $\mathbf{P}_0$, while the last two are proportional to it. The nuclear-magnetic interference scattering σ_I gives a symmetric scattering pattern with respect to the momentum transferred q. The last term σ_{CH} gives rise to the appearance of the left-right asymmetry in scattering, being related to either static or dynamic[25] chirality of the magnetic structure. The three magnetic contributions to the scattering (σ_M, σ_I, and σ_{CH}) may be distinguished and studied in the experiments with polarized neutrons.

In the critical range near the magnetic phase transition σ_N is τ independent and therefore it can be separated from the magnetic scattering σ_M. In a case when the nuclear density fluctuations exist and correlate to the magnetic fluctuations, the nuclear-magnetic interference contribution σ_I occurs. Because the ferromagnets have no static helicoidal (chiral) structure, the last term σ_{CH} arises in presence of a magnetic field as a dynamical contribution, giving the unique possibility to study the critical dynamics of the ferromagnets.[11–13] In a system with a Gaussian distribution of the local Curie temperature, the scattering from spin waves may be significant even around the critical temperature. Although the spin waves are not well defined at $T \approx T_C$, the spin-wave contribution in the chiral dynamical channel should be accounted for in Refs. 14–16. This contribution vanishes when the applied magnetic field $\vec{H}$ is parallel or perpendicular to the incident beam $\vec{k}$. It is unequal to zero only when the magnetic field is inclined to the beam, so-called inclined geometry, having its maximum at the inclination angle $\varphi = 45°$. A detailed description of the SAPNS in inclined geometry for the scattering on the critical fluctuations and on the spin waves is given in the Appendix.

The SANS experiments on the same sample, as described in Sec. II, were carried out at the SANS-2 scattering facility of the FRG-1 research reactor in Geesthacht (Germany). The schematic outline of the experiment is given in Fig. 5. A beam of polarized neutrons with the initial polarization $P_0 = 0.9$, wavelength $\lambda = 0.56$ nm $(\Delta\lambda/\lambda = 0.1)$, and divergence 1.5 mrad was used. The scattered neutrons were detected with a position-sensitive detector with 128×128 pixels within the range $7 \times 10^{-2} \leqslant q \leqslant 7 \times 10^{-1}$ nm^{-1}. The scattering was measured in the temperature range from $T = 450$ K to $T = 600$ K. The external magnetic field of 7–70 mT was applied parallel to the sample long axis at an angle of $\varphi = 45°$, with respect to the incident beam. The adiabatic

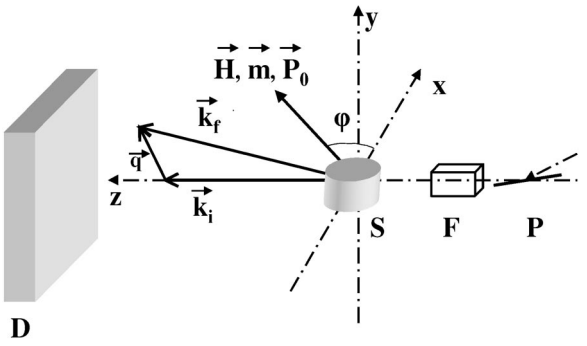

FIG. 5. The schematic outline of SAPNS experiment in the inclined geometry: P is the polarizer, F the spin flipper, S the sample position, and D the two-dimensional position-sensitive detector. The magnetic field $\vec{H}$ is inclined at angle $\varphi=45°$ with respect to the incident beam $\vec{k}_i$ in the (xz) plane.

condition for the transmission of polarized neutrons was sufficiently satisfied to obey the relation $\mathbf{P}_0 \| \mathbf{H}$.

The SANS experiment in a lower magnetic field of 1 G was performed on the multi-detector small-angle polarized-neutron scattering setup Vector at the WWR-M reactor in St. Petersburg Nuclear Physics Institute. The temperature dependence of SANS intensity in the momentum-transfer range of $3\times10^{-2}\leqslant q\leqslant 3\times10^{-1}$ nm^{-1} was measured around the transition with a temperature step of 1 K.

The method of the inclined geometry allows one to distinguish three contributions to the scattering. First, we separated the magnetic critical scattering from the nonmagnetic contribution. Following the standard procedure we determine the pure magnetic scattering by subtracting from the measured intensity the nonmagnetic background at $T\gg T_C$, i.e., $I_m(q,T)=I(q,T)-I(q,600)$. The polarization-dependent part of the scattering, i.e., $\Delta I(q)=I(P_0,q)-I(-P_0,q)$, consists of two terms. One of them is the symmetric term. To

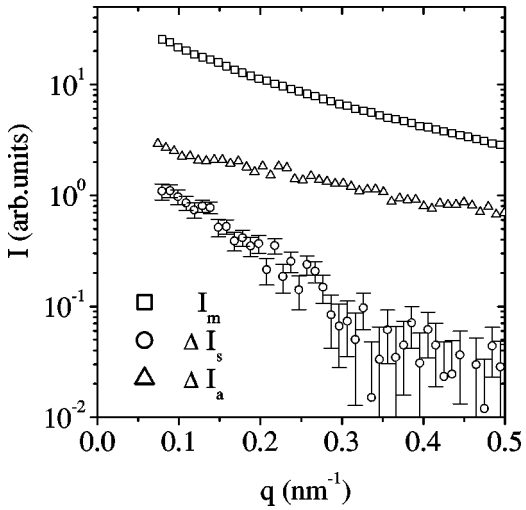

FIG. 6. Three contributions to the magnetic critical scattering measured at $T\simeq\langle T_C\rangle$ as a function of q: the pure magnetic intensity I_m, the antisymmetric polarization-dependent part of the scattering ΔI_a, and the symmetric polarization-dependent part of the scattering ΔI_s.

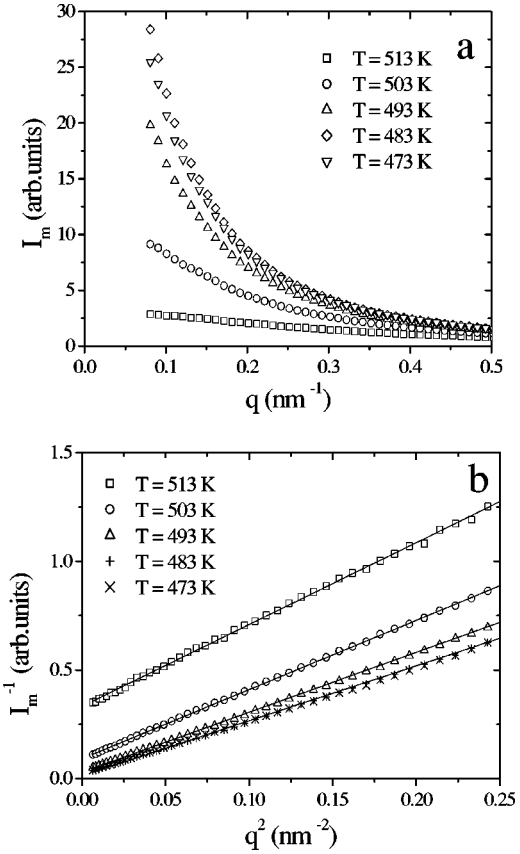

FIG. 7. q dependence of the magnetic scattered intensity I_m (a) and q^2 dependence of I_m^{-1} (b) at different temperatures near T_C.

separate this term from the asymmetric one, we take the difference of the measured intensities $\Delta I(q)$ and average it over 2π at $|q|=\sqrt{q_x^2+q_y^2}$. As a consequence, the antisymmetric part is averaged out and the symmetric part only survives. It is attributed to the nuclear-magnetic interference σ_I. The asymmetry in the scattering is connected with the direction of the magnetic field. In a particular case of $\vec{H}$ being in the (xz) plane (Fig. 5), the asymmetry is most pronounced along the x component of the momentum transfer q_x. Thus the asymmetric contribution was extracted by making the difference of measured intensities $I(\pm P_0,\pm q_x)$:

$$\Delta I_a(q)=\tfrac{1}{4}[I(P_0,q_x)-I(-P_0,q_x)] -\tfrac{1}{4}[I(P_0,-q_x)-I(-P_0,-q_x)]. \quad (4)$$

All three contributions into the scattering are shown as an example in Fig. 6 for $T\simeq\langle T_C\rangle$. Although the symmetric polarization-dependent scattering ΔI_s is about two orders of magnitude smaller than the pure magnetic scattering I_m, it is still well distinguishable. The data on this interference scattering near T_C was published elsewhere.[26]

B. Results: The magnetic scattering

Figure 7(a) gives the q dependence of the magnetic intensity I_m at different temperatures. It is well seen that as the temperature decreases, the magnetic SANS intensity in-

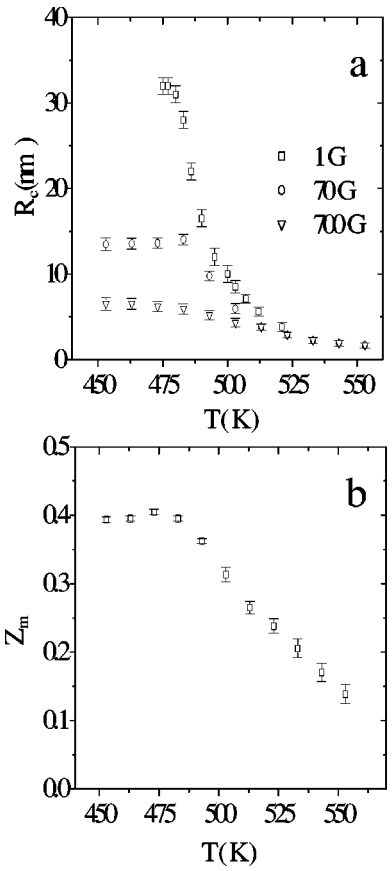

FIG. 8. The temperature dependence of the magnetic correlation length R_c at magnetic fields of 1, 70, and 700 G (a). The value of Z_m as a function of the temperature (b).

creases dramatically at low q while it has a relatively small change at higher q values. This demonstrates an appearance of critical fluctuations with a correlation length of about 10 nm in this temperature range. It is important to note that the growth in the intensity saturates with decreasing temperature at $T \approx 485$ K. The inverse intensity I_m^{-1} is plotted in Fig. 7(b) as a function of q^2 in order to verify validity of the Ornstein-Zernike expression

$$I_m(q) = \frac{Z_m}{q^2 + \kappa_c^2}, \tag{5}$$

where $\kappa_c = R_c^{-1}$ is the inverse correlation length. All data sets show the linear dependence of I_m^{-1} on q^2.

The temperature dependence of parameters Z_m and κ_c^2 has been obtained from a least-squares fit to the data with Eq. (5) convoluted with the apparatus resolution function with its spread of 3×10^{-2} nm^{-1}. The correlation length of the critical fluctuations $R_c = \kappa^{-1}$ at different magnetic field H is presented in Fig. 8(a). First, it increases as temperature decreases at $T > 485$ K and then becomes almost constant. The value of Z_m demonstrates a smooth growth with decreasing temperature and saturates at $T \approx \langle T_C \rangle = 485$ K [Fig. 8(b)]. Z_m does not depend on the magnetic field. The correlation length R_c does not appear to get infinitely large at $T = T_C$.[27,28] This may be caused by the resolution effect.

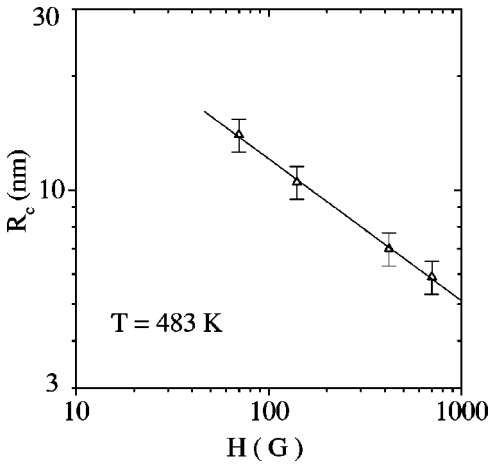

FIG. 9. The magnetic-field dependence of the correlation length R_c at $T = 483$ K.

As seen in Fig. 8, the magnetic field strongly affects the correlation length R_C. At the same time parameter Z_m shows no field dependence. At a relatively large field of $H = 700$ G the temperature dependence of R_c tends to disappear. The strong effect of the field on R_c is more pronounced as far as the temperature approaches T_C from above in the range $\tau \leqslant \Delta T_C / T_C \approx 0.05$, or within the range of the T_C variations. The decrease in the correlation length R_c, in a magnetic field, indicates the enhancement of homogeneity in the magnetically fluctuating system. It should be noticed that the magnetic field of 10–1000 G does not produce any anisotropy in the intensity of quasielastic scattering in the plane of 2D detector. We therefore used an average value of the intensity at $|q| = \sqrt{q_x^2 + q_y^2} = \text{const}$.

The effect of the magnetic field on the correlation length of the critical fluctuations can be understood in terms of the balance between energy of the magnetic field $g\mu H$ and that of the critical fluctuations $T_C(\kappa a_0)^Z$, where $Z = 5/2$ and a_0 is a lattice constant of order 0.1 nm (Refs. 29 and 30) (see also the Appendix). For $g\mu H \gg T_C(\kappa_{(H=0)} a_0)^Z$, the correlation length is renormalized as a function of the magnetic field: $\kappa(H) a_0 = (g\mu H / T_C)^{1/Z}$. The high-field limit is obeyed for all measured data points at $T = 483$ K. Figure 9 shows the field dependence of the correlation length at $T = 483$ K. A fit of the data gives $Z = 2.63 \pm 0.07$ with $a_0 = 0.140 \pm 0.005$ nm, which is very close to the theoretical value of $Z = 5/2$.

The observed renormalization of $\kappa_c(H)$ indicates that for $q \leqslant \kappa_c(H)$ the energy of the critical fluctuations $\Omega = T_C(\kappa_H a_0)^{5/2}$ is determined by the field H. While for $q \geqslant \kappa(H)$ the energy is equal to $\Omega_c = T_C(q a_0)^{5/2}$ and the magnetic field should be considered as a weak perturbation.

C. Results: The chiral scattering

In this section we show the data which can be attributed to the antisymmetric part of the dynamic susceptibility. It is well known that the neutron magnetic scattering is determined by two-spin-correlation function, which is connected to the imaginary part of the conventional spin susceptibility.

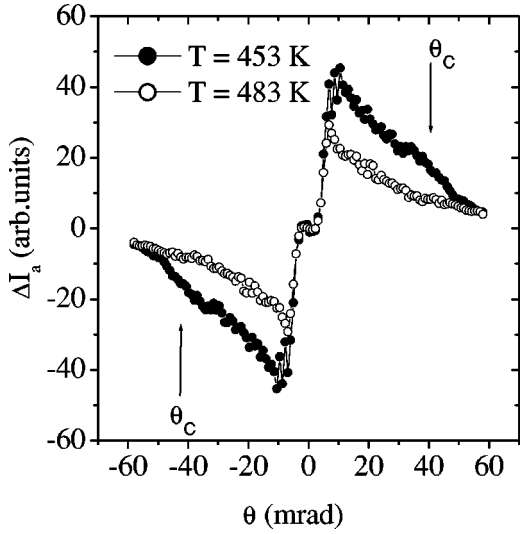

FIG. 10. The q dependence of the asymmetric part of the SAPNS ΔI_a for the magnetic field of $H=700$ G at $T=453$ and 483 K. The arrows show features attributed to the cutoff angle θ_C in the neutron scattering from spin waves.

In zero magnetic field it is a symmetric second-rank tensor and the neutron-scattering intensity does not depend on the neutron polarization. In magnetic field the antisymmetric part appears and if the field is along the z direction we have $\langle S_x S_y\rangle \neq \langle S_y S_x\rangle$ and the cross section becomes dependent on $\mathbf{P}_0$. In weak field this antisymmetric part is proportional to the field $\mathbf{H}$, and as the Zeeman interaction is a product of $\mathbf{H}$ and the total spin $\Sigma \mathbf{S}_R$ it is a three-spin-correlation function.[13,25] At $T<T_C$ for unidomain sample instead of $\mathbf{H}$ we have the total magnetization, and the spin-wave absorption and excitation are related to the components $\langle S_- S_+\rangle$ and $\langle S_+ S_-\rangle$ of the susceptibility tensor, respectively, where $S_\pm = S_x \pm i S_y$ (see also the Appendix for details).

The data below demonstrate how the spin excitations at $T\sim T_C$ transform into spin waves in the ferromagnetic state. Figure 10 shows the asymmetric polarization-dependent part of the scattering ΔI_a. The central part of the picture is shadowed by the beam stop. The shape of the pattern $\Delta I(\theta)$ changes with the temperature as shown for $T<T_C$ and for $T\sim T_C$. At $T<T_C$ one can clearly distinguish the feature at $\theta\sim 40$–50 mrad. This feature is attributed to the cutoff angle in the neutron scattering from spin waves, which, according to Eq. (A2) is given by $\theta_c^2=\theta_0^2-gm_BH/Dk^2$, where $\theta_0 = E/Dk^2$ and D is the spin-wave stiffness. At $T\sim T_C$, this cutoff angle becomes hardly distinguishable, showing that spin waves become heavily damped.

To provide a quantitative analysis for the data, it is convenient to describe the asymmetric scattering in terms of the ''polarization''

$$P_a(\theta)=\Delta I_a(\theta)/I_m(\theta), \tag{6}$$

where $I_m(\theta)$ is the magnetic scattering. The analytical expression for P_a in case of critical fluctuations is given by [Eq. (A8)]

$$P_a = AP_0 \frac{g\mu_B H}{E}\frac{k}{\kappa}\mathrm{sgn}(\theta)\sin 2\varphi. \tag{7}$$

The expression is valid within the range $\kappa<k\theta<q_c$, where $q_c=a^{-1}[2E/(T_C ka)]^{2/3}$ is the inelastic characteristic momentum for the critical fluctuation. It is about 1.5 nm^{-1} in our case. The remarkable features of this function are the following.

(1) It appears only when the inclination angle φ between the magnetic field $\vec{H}$ and the incident beam direction $\vec{k}$ is not equal to 0 or $\pi/2$. Its appearance in this inclined geometry implies the dynamical nature of the scattering.

(2) The function changes its sign for the positive and negative values of the scattering angle θ.

(3) It does not depend on θ itself.

(4) It depends linearly on the value of the applied magnetic field H.

(5) It vanishes for the nonpolarized neutrons ($P_0=0$).

The expression for the chiral scattering from spin waves is given as [Eq. (A12)]

$$\sigma_{ch}(\theta)=-r^2\langle S\rangle P_0(T/E)(\theta_0/\theta)(\theta_0^2-\theta^2)^{-1/2}\sin 2\varphi. \tag{8}$$

Here θ_0 is the cutoff angle for neutron scattering on spin waves. We neglect an effect of the magnetic field since $(g\mu_b H)/E<3\times10^{-3}\ll\theta_0\sim 50\times10^{-3}$ in our experiment. The features of this scattering are as follows:

(1) it appears only in inclined geometry $\varphi\neq 0,\pi/2$;

(2) it is an odd function of the scattering angle θ;

(3) it is proportional to the magnetization $\langle S\rangle$; and

(4) it vanishes for $P_0=0$.

The expression [Eq. (8)] may be further simplified in the approximation of a large θ_0 (or small spin-wave stiffness D), which is rather well fulfilled in the vicinity of T_C. Thus for $(\theta/\theta_0)^2\ll 1$ and after normalization on the magnetic scattering, where we have assumed for $I_m(\theta)=A_m^2(k\theta)^{-2}$, we have

$$P_a(\theta)=\langle S\rangle P_0(T/E)\,\theta\sin 2\varphi. \tag{9}$$

Figure 11 shows typical examples of the polarization $P_a(k\theta)$ as a function of (a) the magnetic field and (b) the temperature. As seen from Fig. 11, the slope of the linear dependence increases as the temperature decreases. The experimental data for P_a at $k\theta>\kappa$ have been fitted to $P_a = P_a^0+\alpha k\theta$. The parameter P_a^0 does not depend on the temperature and is found to be proportional to magnetic field (Fig. 12). The parameter α saturates quickly with the field. The saturation value α_s decreases as the temperature increases (Fig. 13). The two parameters, describing the function P_a, differently depend on the temperature and magnetic field. Thus, we conclude that the measured value of P_a consists of two contributions: scattering from the spin waves in the large magnetic inhomogeneities, which align along the field at low H, and the scattering from the three-spin critical correlations inside the critical region. The part of the function P_a (P_a^0), which is proportional to H, is attributed to the three-spin correlations inside the critical fluctuations [Eq.

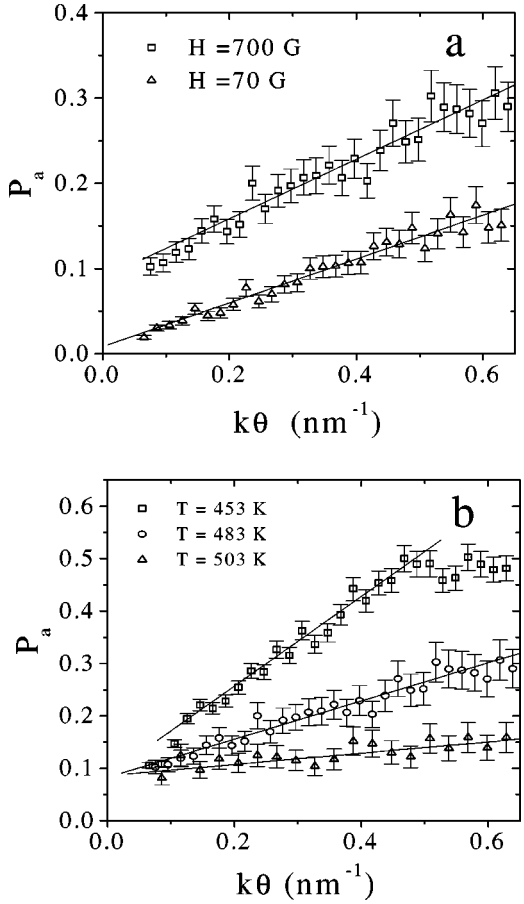

FIG. 11. The polarization $P_a(k\theta)$ in a magnetic field of $H=70$ and 700 G at $T=483$ K (a) and at a temperature of $T=453$, 483, and 503 K at $H=700$ G (b).

(7)]. It is also supposed to be θ independent, so that $\Delta I_a \sim \theta^{-2}$ as well as the pure magnetic scattering $I_m \sim q^{-2}$ in the range $K\theta > \kappa$. This behavior is in agreement with the principle of the dynamical critical factorization, which is known as Poliakov-Kadanoff-Wilson algebra (see the Appendix and Ref. 17). The expression of P_a for the spin waves is not proportional to the magnetic field H but rather to the magnetization $\langle S \rangle$, which is saturated in a magnetic field of 100 G. This behavior is clearly demonstrated by the second contribution [$\alpha(k\theta)$] to the experimental curve P_a. Therefore one may identify α with $\langle S \rangle (T/E)$. As a result the T dependence of α_s should be the same as for $\langle S \rangle T$, when averaged over the spatial distribution of the large-scale inhomogeneities. The corresponding curve in Fig. 13 shows the function

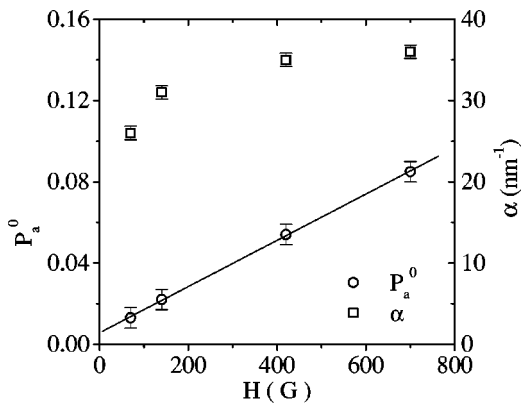

FIG. 12. The magnetic-field dependence of P_a^0 and α.

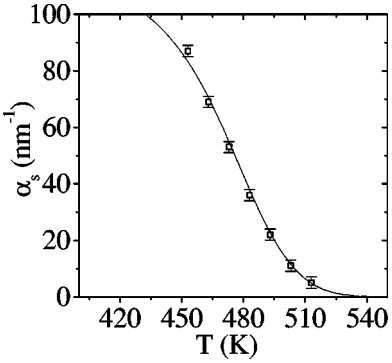

FIG. 13. The temperature dependence of the parameter α_S. The solid line is the fit to the data (see text).

$$F(T) \sim T \int_T^\infty \rho(T_C) M(T, T_C) dT_C ,$$

with parameters for $\rho(T_C)$ taken as $T_C = 485$ K and $\Delta T_C = 20$ K. Thus the existence of spin waves is observed in the temperature range $T_C - \Delta T_C < T < T_C + \Delta T_C$, where both ferromagnetic and paramagnetic regions coexist. It should be noted that the width of the probability function $\rho(T_C)$ for this data set is larger than that for the neutron depolarization. A possible reason for this may be the larger magnetic field of 700 G applied in the former case compared with 50 G in the latter case.

IV. CONCLUDING REMARKS

The magnetic-phase transition in the invar $Fe_{65}Ni_{35}$ alloy has been investigated. We have combined the results of small-angle polarized-neutron scattering with both three-dimensional neutron depolarization and thermal-expansion measurements. The main results are as follows.

(1) It is interesting to combine two different correlation lengths obtained by ND and SANS methods. A relatively small length scale R_c (with a Lorentzian shape), which is studied by SANS, is attributed to critical fluctuations. The ND measurements also show the presence of large-scale inhomogeneities R_d with a ''squared'' Lorentzian shape.[6] Figure 14 demonstrates the real coexistence of two characteristic length scales in the temperature region around the ferromagnetic transition temperature T_C. Only the limitations of two different methods do not allow one to observe them both simultaneously in one method. SANS is restricted at low values of q by resolution at 0.01 nm^{-1}, therefore, it is insensitive for a relatively large inhomogeneity, while the neutron depolarization method is restricted by the sensitivity for a relatively small magnetic inhomogeneity, which is strongly connected with the neutron wavelength. It is also worthwhile to note that the ND method is practically insensitive to the critical fluctuations with a Lorentzian shape.[6]

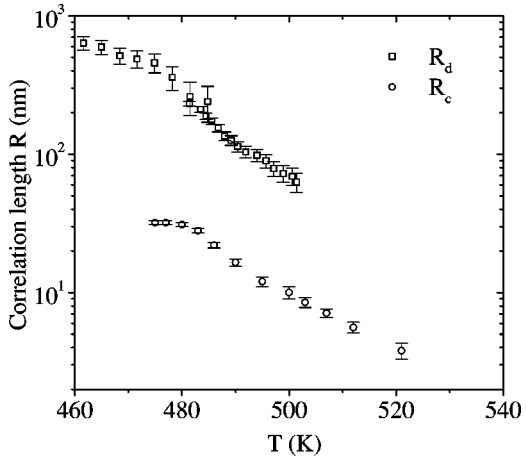

FIG. 14. The combined plot of the correlation lengths R_c for the critical fluctuations and R_d for the T_C variations as a function of the temperature.

(2) To interpret the neutron depolarization data we introduce a spatial variation in the Curie temperature T_C, which fluctuates around an average value $\langle T_C \rangle$.[7] The local T_C variations are described by a standard deviation of the transition temperature ΔT_C and by the characteristic correlation length $R_0 \sim R_d(\langle T_C \rangle)$. The deduced parameters are $\langle T_C \rangle = 485 \pm 0.5$ K, $\Delta T_C = 12.5 \pm 0.2$ K, and $R_0 \approx 3 \times 10^3$ Å. The important point of the description proposed above concerns the strength of the applied magnetic field, which is able to reveal the average magnetization of the sample. A weak magnetic field must be held in order to probe large-scale inhomogeneities. Intuitively the condition is the following: the applied magnetic field is sufficiently strong to move the domain walls inside the ferromagnetic regions, but is weak in comparison with the anisotropy field ($\omega_0 \langle S \rangle < g\mu_b H < K$). Here ω_0 is the energy of dipole interaction (0.1 meV) for this system and K is anisotropy constant. For the critical range this condition is sufficiently fulfilled for the field strength of 50–100 G. It is also important that the field does not create new magnetic inhomogeneities in this system with large magnetostriction and a strong spin-lattice coupling.

(3) The strong magnetoelastic coupling may result in the appearance of superparamagnetic regions above T_C, which are then transformed into the ferromagnetic clusters/inhomogeneities. The measured changes in the sample length near the transition were interpreted in accordance with the concept of this variation in T_C. Although the parameters for the distribution in T_C obtained from the TE measurements are close to those derived from the ND measurements, they cannot be explained within the range of T_C variations and requires the presence of critical fluctuations. Therefore, we conclude that the magnetic expansion of the sample, resulting in the invar behavior, occurs also above T_C inside the critical fluctuations.

(4) The SAPNS measurements were performed in a magnetic field **H** using a special inclined geometry (**H** is inclined to the wave vector **k**). Two contributions to the critical scattering were studied at different magnetic fields (10–1000 G) for temperatures around T_C. First, the pair spin-correlation function was deduced with their amplitude and the correlation length $R_c(T,H)$. T_C variations on correlation length R_c of the critical fluctuations lead to the fact that R_c does not appear infinitely large at $T = T_C$. The length R_c is assumed not to be unique and is averaged over the T_C variations, so that one can estimate a maximum value of $R_c \sim a\tau_0^{-\nu}$, where $\tau_0 = \Delta T_C / \langle T_C \rangle$. In spite of the fact that the phase transition is smeared by T_C variations, the crossover to the strong-field regime in the critical temperature range is observed. Thus the temperature dependence of R_c tends to disappear in a large field limit. The correlation length is suppressed by the magnetic field as $R_c(H) = a_0 (g\mu H / T_C)^{1/Z}$ with $a_0 = 0.140 \pm 0.005$ nm and $Z = 2.63 \pm 0.07$, which is very close to the theoretical value of $Z = 5/2$.

(5) Another part of the critical scattering was investigated by extracting the asymmetric part of the polarization-dependent scattering. This scattering appears only in inclined geometry and implies the dynamical (chiral) nature of the scattering. We distinguish two contributions in the asymmetric scattering, which stem from the spin waves in the large magnetic inhomogeneities and from the three-spin correlations in the critical fluctuations. The picture of the critical dynamical (chiral) scattering can be understood within the framework of our model of T_C variations.

ACKNOWLEDGMENTS

We thank N. Geerlofs for performing the thermal-expansion measurements. The PNPI-team acknowledges GKSS for their hospitality. Russian authors thank for partial support RFBR (Grant Nos. 03-02-17340, 01-02-17286, and 04-02-16342, SS-1671.2003.2), Grant Goscontract Contract No. 40.012.1.1.1149, and Russian state programs ''Collective and Quantum Effects in Condensed Matter,'' ''Quantum Macrophysics,'' and ''Neutron Research of Solids.''

APPENDIX: SAPNS IN THE "INCLINED" GEOMETRY

In the case of a disordered system with T_C fluctuations with a spread of ΔT_C around an average value $\langle T_C \rangle$, both paramagnetic and ferromagnetic regions coexist within the temperature range $T_C - \Delta T_C < T < T_C + \Delta T_C$. In the paramagnetic regions we have critical fluctuations, which are described by the dynamical scaling. In the ferromagnetic regions one should consider the spin-wave excitations. We present below the theoretical description of the polarized-neutron scattering for both parts following Refs. 13 and 25.

The dynamical chiral scattering appears if the system is either in an external magnetic field or has a spontaneous magnetization. In the former case of a weak magnetic field it is described by three-spin-correlation function. In the latter case it is scattering caused by spin waves. For the small-angle scattering the chiral cross section has the following form:[13,25]

$$\sigma_{ch}(\mathbf{q},\omega) = (2rP_0T/\pi\omega)(\hat{q}\cdot\hat{h})^2 \ \mathrm{Im}\ C(\mathbf{q},\omega), \quad \text{(A1)}$$

where $\hat{h}$ and $\hat{q}$ are unit vectors along magnetic field **H** and momentum transfer **q**, respectively, and ω is the energy

transfer. In this expression we have taken into account that both the dynamical chirality $\mathbf{C}(\mathbf{q},\omega)$ and the neutron polarization $\mathbf{P}_0$ are directed along the field, and $\mathbf{C}=\mathbf{h}C$.

In our experimental device we integrate over all energies of the scattering neutrons. According to Refs. 13 and 25 the Im $C(\mathbf{q},\omega)$ is an even function of ω and therefore the integrated chiral cross section should be zero, if there is no ω-odd term in the factor $(\hat{h}\cdot\hat{q})^2$ [see Eq. (A1)]. Such ω-odd term appears if the magnetic field $\mathbf{H}$ is inclined with respect to the incident beam at the angle φ (Fig. 5). As $q_x=k\theta$ and $q_z=k\omega/(2E)$, where k and E are the incident neutron momentum and the incident energy, respectively, we have

$$(\hat{q}\cdot\hat{h})^2=\frac{(2E\theta)^2\cos^2\varphi+\omega^2\sin^2\varphi+2E\theta\omega\sin 2\varphi}{(2E\theta)^2+\omega^2}. \tag{A2}$$

Here the third term is ω-odd and the ω-integrated chiral cross section is given by

$$\sigma_{ch}(\theta)=2r^2P_0\frac{T}{\pi}\int_{-\infty}^{\infty}\frac{d\omega 2E\theta\,\mathrm{Im}C(\mathbf{q},\omega)}{(2E\theta)^2+\omega^2}\sin 2\varphi. \tag{A3}$$

This integral can be evaluated in two limiting cases: (1) critical paramagnetic region and (2) spin-wave region below T_C.

(a) *Critical paramagnetic region*. It is defined by the following conditions: $T>T_c$ and $q\gg\kappa$, where κ is the inverse correlation length of the critical fluctuations defined as $\kappa=\tau^{\nu}/a$, where $\tau=|T-T_c|/T_c$ is a reduced temperature, $\nu\approx 2/3$ is the critical exponent of the correlation length, and a is of the order of the lattice spacing.

In the scaling theory of phase transitions all physical variables have scaling dimensionalities, which determine the general form of the corresponding correlation function. For example, the two-spin-correlation function has the form

$$G(q)=\frac{1}{(\kappa a)^{2-\eta}}F\left(\frac{q}{\kappa}\right)=\frac{Z}{a^2(q^2+\kappa^2)}, \tag{A4}$$

where the right-hand Ornstein-Zernicke expression holds if $\eta\ll 1$, as it is the case ($\eta<0.1$), and we will neglect η below.

For the magnetic field we have the condition that $g\mu_BH/T_c(\kappa a)^{5/2}=f$ is a dimensionless number. If $f\ll 1$ the field is weak. For $f\gg 1$ we have the strong-field regime and get $\kappa=(g\mu_BH/T_c)^{2/5}$, i.e., κ becomes τ independent.

In a weak field the chiral scattering has to be proportional to $\mathbf{H}$. So its scaling dimensionality is determined by the product $G(q)f$ and we get

$$\mathrm{Im}C(q,\omega)=\frac{g\mu_BH}{T_c(\kappa a)^{9/2}}F\left[\frac{q}{\kappa},\frac{\omega}{\Omega(q)}\right], \tag{A5}$$

where $\Omega(q)=T_c(qa)^{5/2}$ is the characteristic energy of the critical fluctuations with momentum $\mathbf{q}$, which is valid for ferromagnets in the exchange approximation.[29,30]

The dynamical chirality is the three-spin-correlation function and it may be considered as a result of the scattering of the critical fluctuation on the uniform magnetic field.[25] From this point of view it is clear that really $C(\mathbf{q})$ is a function of two momenta: $\mathbf{q}$ and a momentum of the field $\mathbf{q}_H=0$. In Ref. 17 was formulated a principle of critical factorization, which is known as Polyakov-Kadanoff-Wilson Operator algebra. It states that in any multispin-correlation function the dependence on the largest momentum $\mathbf{q}$ ($q\gg\kappa$) appears as a factor $(q/\kappa)^{-5+1/\nu}\Phi[\omega/\Omega(q)]$. In our case, putting $\nu\approx 2/3$ we get

$$\mathrm{Im}C(q,\omega)=\frac{g\mu_BH}{T_c(qa)^{7/2}(\kappa a)}\Phi\left[\frac{\omega}{\Omega(q)}\right]. \tag{A6}$$

In this expression we have $q=k[\vartheta^2+(\omega/2E)^2]^{1/2}$. The dependence of $\mathbf{q}$ on ω may be neglected in quasielastic case, when the time, which neutron spends in the space region of the order of $1/q$, is much less than the characteristic time of the fluctuation with the same size $\hbar/\Omega(q)$. The corresponding condition has the form

$$q\ll q_{in}=a^{-1}(2E/T_cka)^{2/3}. \tag{A7}$$

In this case we can replace $\mathbf{q}$ by $k\vartheta$ and neglect ω in the denominator of Eq. (A3). As a result the ratio of the chiral cross section to the conventional one, Eq. (A4), is given by[13]

$$\frac{\sigma_{ch}(\theta)}{\sigma(\theta)}=AP_0\frac{g\mu_BH}{E}\frac{k}{\kappa}\mathrm{sgn}(\theta)\sin 2\varphi \tag{A8}$$

Here A is a constant of the order of unity. Experimentally this expression was confirmed for critical scattering in iron.[31]

(b) *Spin-wave region*. The chiral vector $\mathbf{C}(\mathbf{q},\omega)$ determines antisymmetric part of the spin susceptibility

$$\chi_{\alpha\beta}=\chi^{(S)}_{\alpha\beta}-i\epsilon_{\alpha\beta\gamma}C_{\gamma}, \tag{A9}$$

where $\chi^{(S)}_{\alpha\beta}$ is the symmetric part of the susceptibility and $\epsilon_{\alpha\beta\gamma}$ is the antisymmetric unit pseudotensor. Then using standard spin-wave theory[32] and taking into account that spins are aligned against magnetization we get

$$\mathrm{Im}\,C(\mathbf{q},\omega)=-(\pi\langle S\rangle/2)[\delta(\omega-\epsilon_{\mathbf{q}})+\delta(\omega+\epsilon_{\mathbf{q}})], \tag{A10}$$

where $\langle S\rangle>0$ is the average lattice spin and $\epsilon_{\mathbf{q}}=g\mu_BH+Dq^2$ is the spin-wave energy. Substituting this expression into Eq. (A3) we obtain after some calculations

$$\sigma_{ch}(\theta)=-r^2\langle S\rangle\sin 2\varphi P_0\frac{T}{E}\frac{\theta\theta_0}{(\theta_0^2-\theta^2-g\mu_bH/Dk^2)^{1/2}}\times\frac{\theta_0^2-(g\mu_bH/2Dk^2)}{\theta_0^2\theta^2+(g\mu_bH/2Dk^2)^2}, \tag{A11}$$

where $\theta_0=E/Dk^2$. At $H=0$ we get

$$\sigma_{ch}(\theta) = -r^2\langle S\rangle P_0(T/E)(\theta_0/\theta)(\theta_0^2-\theta^2)^{-1/2}\sin 2\varphi. \qquad \text{(A12)}$$

For a complete analysis we need also the expression for the conventional spin-wave cross section. We give it for $\varphi = 45°$ only. In this case we have

$$\sigma(\theta) = 3r^2\langle S\rangle(T/2E)\frac{\theta_0^4}{\theta^2+(g\mu_B H/Dk^2)} \times \frac{1}{[\theta_0^2-\theta^2-(g\mu_B H/Dk^2)]^{1/2}}. \qquad \text{(A13)}$$

*Email address: grigor@pnpi.spb.ru

[1] S.R. Andrews, J. Phys. C **19**, 3721 (1986).
[2] R.A. Cowley, Phys. Scr. **66**, 24 (1996).
[3] K. Hirota, G. Shirane, Q.J. Harris, Q. Feng, R.J. Birgeneau, M. Hase, and K. Uchinokura, Phys. Rev. B **52**, 15 412 (1995).
[4] A.Yu. Romanov, V.P. Silin, and D. Wagner, Phys. Lett. A **226**, 310 (1997).
[5] A.Yu. Romanov and V.P. Silin, Zh. Eksp. Teor. Fiz. **113**, 213 (1998) [JETP **86**, 120 (1998)].
[6] A.L. Korzhenevskii, H-O. Heuer, and K. Herrmanns, J. Phys. A **31**, 927 (1998).
[7] A.L. Korzhenevskii, K. Herrmanns, and H.-O. Heuer, Europhys. Lett. **45**, 195 (1999).
[8] S.V. Grigoriev, S.V. Maleyev, A.I. Okorokov, and V.V. Runov, Phys. Rev. B **58**, 3206 (1998).
[9] S.V. Grigoriev, S.A. Klimko, W.H. Kraan, S.V. Maleyev, A.I. Okorokov, M.Th. Rekveldt, and V.V. Runov, Phys. Rev. B **64**, 094426 (2001).
[10] S.L. Ginzburg, Zh. Eksp. Teor. Fiz. **70**, 1961 (1977) [Sov. Phys. JETP **46**, 1029 (1977)].
[11] A.I. Okorokov, A.G. Gukasov, V.V. Runov, and M. Roth, Solid State Commun. **38**, 583 (1981).
[12] A.I. Okorokov, A.G. Gukasov, V.V. Runov, M. Roth, and V.E. Mikhailova, Zh. Eksp. Teor. Fiz. **81**, 1462 (1981) [Sov. Phys. JETP **51**, 775 (1981)].
[13] A.V. Lazuta, S.V. Maleyev, and B.P. Toperverg, Zh. Eksp. Teor. Fiz. **81**, 2095 (1981) [Sov. Phys. JETP **54**, 1113 (1981)]; Solid State Commun. **38**, 589 (1981).
[14] A.I. Okorokov, V.V. Runov, B.P. Toperverg, A.D. Tret'yakov, E.I. Mal'tsev, I.M. Puzeii, and V.E. Mikhailova, Pis'ma Zh. Eksp. Teor. Fiz. **43**, 390 (1986) [JETP Lett. **43**, 503 (1986)].
[15] V. Deriglazov, A. Okorokov, V. Runov, B. Toperverg, R. Kampmann, H. Eckerlebe, W. Schmidt, and W. Lobner, Physica B **181-182**, 262 (1992).
[16] B.P. Toperverg, V.V. Deriglazov, and V.E. Mikhailova, Physica B **183**, 326 (1993).
[17] A.M. Polyakov, Zh. Eksp. Teor. Fiz. **57**, 271 (1969) [Sov. Phys. JETP **30**, 151 (1970)].
[18] R. Rosman and M.Th. Rekveldt, Phys. Rev. B **43**, 8437 (1991).
[19] R. Rosman and M.Th. Rekveldt, J. Magn. Magn. Mater. **95**, 319 (1991).
[20] S.V. Grigoriev, W.H. Kraan, S.V. Maleyev, A.I. Okorokov, M.Th. Rekveldt, and V.V. Runov, J. Neutron Res. **8**, 155 (2000).
[21] S.V. Grigoriev, V.V. Runov, A.I. Okorokov, O.A. Gubin, G.P. Kopitsa, A.D. Tretiakov, and M.K. Runova, Nucl. Instrum. Methods Phys. Res. A **389**, 441 (1997).
[22] V.L. Sedov, *Antiferro-Magnetism of γ-Iron*: *The Invar Problem* (Nauka, Moscow, 1987).
[23] S.V. Maleyev, V.G. Bar'yakhtar, and R.A. Suris, Fiz. Tverd. Tela (Leningrad) **4**, 3461 (1962); Sov. Phys. Solid State **4**, 2533 (1963).
[24] M. Blume, Phys. Rev. **130**, 1670 (1963).
[25] S.V. Maleyev, Phys. Rev. Lett. **75**, 4682 (1995); A. Gukasov, Physica B **267-268**, 97 (1999); S.V. Maleyev, *ibid.* **297**, 67 (2001); Usp. Fiz. Nauk **172**, 617 (2002) [Phys. Usp. **46**, 569 (2002)].
[26] S.V. Grigoriev, S.V. Maleyev, A.I. Okorokov, and H. Eckerlebe, Europhys. Lett. **63**, 56 (2003).
[27] R.A. Cowley, G. Shirane, R.J. Birgeneau, E.C. Svensson, and H.J. Guggenheim, Phys. Rev. B **22**, 4412 (1980).
[28] G. Aeppli, S.M. Shapiro, R.J. Birgeneau, and H.S. Chen, Phys. Rev. B **28**, 5160 (1983).
[29] S. Ma, *Modern Theory of Critical Phenomena* (Benjamin, New York, 1976).
[30] S.V. Maleyev, in *Physics Review*, edited by I.M. Khalatnikov (Harwood Academic, Chur, 1987), Vol. 8, p. 323.
[31] A.I. Okorokov, A.G. Gukasov, V.N. Slusar, B.P. Toperverg, O. Schärpf, and F. Fuzhara, Pis'ma Zh. Eksp. Teor. Fiz. **37**, 269 (1983) [JETP Lett. **37**, 319 (1983)].
[32] A.I. Ahiezer, V.G. Bar'yakhtar, and S.V. Peletminskii, *Spin Waves* (North-Holland, Amsterdam, 1968).